Velocity-Aided IMU-Based Tilt and Attitude Estimation

Mehdi Benallegue, Abdelaziz Benallegue, Rafael Cisneros, Yacine Chitour

Velocity-aided IMU-based Tilt and Attitude Estimation

Mehdi Benallegue, Abdelaziz Benallegue, Rafael Cisneros, Yacine Chitour

***Abstract*—This paper addresses the problem of estimating the tilt and more generally the attitude of a rigid body that is subject to high accelerations and equipped with inertial measurement units (IMU) and a sensor providing the body velocity (expressed in the reference frame attached to the body). In the absence of a magnetometer, tilt estimation is proposed through a two-step observer: a global-exponentially stable pre-estimation given to a manifold-constrained complementary filter. In the presence of a magnetometer, the presented observer allows to reconstruct the full attitude and tune how much the estimation of the tilt is influenced by the magnetometer, depending on the level of confidence given to the measurements of the magnetometer. All state estimators are proposed with proofs of almost global asymptotic stability and local exponential convergence. Finally, these estimators are compared with state-of-the-art solutions in clean and noisy simulations, allowing recommended solutions to be drawn for each case.**

I. Introduction

The orientation, or attitude, of a mechanical system in the world, is often an important part of its dynamical state. More specifically, the orientations on Earth can be split into two components: first, the "tilt", lying in a 2D manifold, representing the deviation of the local vertical axis of the robot with regard to the world's global gravitational field direction, and second the remaining variable lying in a 1D manifold that represents the heading around the world's gravitational field and that is often called "yaw", though this definition is local and singularity-prone. This decomposition is relevant because in the majority of robotic systems the dynamics are invariant about yaw but are tied closely to tilt. For instance, tilt constitutes sometimes the most important variable determining the dynamics such as in the case of drones [10] or legged robots [28], because it deeply determines balance and stability. Thus, tilt references usually need to be tightly tracked and their estimation is required at high frequency and precision and is used in high gain feedback control loops. In these cases, yaw is often used only for navigation and does not require the same level of frequency and precision as those needed for tilt estimation.

M. Benallegue, A. Benallegue and R. Cisneros are with CNRS-AIST JRL (Joint Robotics Laboratory), IRL, and National Institute of Advanced Industrial Science and Technology (AIST) Japan. A. Benallegue is also with Université Paris-Saclay, UVSQ, Laboratoire d'Ingénierie des Systèmes de Versailles, 78124, Vélizy -Villacoublay, France. Y. Chitour is with Université Paris-Saclay, CNRS, CentraleSupélec, Univ. Paris-Sud, Laboratoire des Signaux et Systèmes, 91190, Gif-sur-Yvette, France. mehdi.benallegue@aist.go.jp, abdelaziz.benallegue@uvsq.fr, rafael.cisneros@aist.go.jp, yacine.chitour@lss.supelec.fr

While it is possible for fixed-based robots to reconstruct the orientation of any link using the joint position, this is not possible for mobile robots, specifically floating-base ones. These robots often resort to state observation techniques relying on the measurements obtained using various kinds of sensors. The most prominently used set of sensors is called the inertial measurement unit (IMU), which measures the linear acceleration, including the gravitational one, the angular velocity, and sometimes the magnetic field measurement, all expressed in the frame of the sensor. The measurements of the magnetic field are usually intended to exploit the Earth's magnetic field to contribute to the attitude estimation, however, they are likely to suffer from the presence of noise and are often considered less reliable than the two other measurements [21]. Nevertheless, in several cases, the magnetic field measurements are unnecessary to estimate the tilt alone. In these cases, yaw estimation is used mostly for navigation and exploits lower performance sensors such as GPS, and computer vision, or is even absent in the case of teleoperated robots. Nonetheless, if the magnetic field measurements are available and reliable, they provide a better estimation, including for tilt.

Using only this set of two or three measurements, an efficient estimation for the tilt or attitude can be built, but under the assumption that the system has negligible linear accelerations compared to gravity [16], [18]. This assumption limits the motions to low dynamics trajectories or is simply impossible to hold, especially when the system is subject to impacts such as during the case of bipedal walking. A dynamical model of the system can be used to predict the accelerations and compensate for them. This prediction can be based on the forces models, either in the case of unmanned aerial vehicles [19], [20] or legged robots [8], [22]. However, this solution is specific to every dynamical system and requires identifying many dynamical parameters.

Another solution is to "aid" the inertial measurement unit (IMU) with independent measurements able to clear the acceleration ambiguity, such as the position in the world frame provided by GPS [13], [24] or linear velocity, either expressed in the world frame [17], [11], the local frame of the sensor [15], [2], [4], or a mixture of both [14], sometimes while reconstructing the velocity itself [1].

It is important to note that there is a deep difference between the cases where the velocities are expressed in the local frame and the case where they are expressed in the global frame: in terms of system dynamics and in terms of observable states and observability conditions. In this work, we assume that the velocity *in the sensor local frame* is available.

II. Problem statement

A. Context

When the velocity in the local frame is available in addition to the IMU one can reconstruct the attitude efficiently with proven Lyapunov convergence. This velocity can be provided by a sensor such as Doppler effect radars. It can be provided also by the measurements of the angular rate in the presence of a known anchor in the environment. This is for example the case of humanoid robots in contact with the environment because the contact point position and velocity in the sensor frame are known [27], [5]. There are a few estimators considering the same case. In [27] an extended Kalman filter is used to perform the fusion between an estimation of the linear velocity of the IMU and its measurements to produce tilt (roll and pitch angles) estimation of a small-size humanoid robot, however, no proof of global convergence was provided. In [2] a velocity-aided estimator with proof of convergence has been presented, but there were possible cases of singularities if the scaling factor reaches zero. In [15] two estimators with proof of convergence have been presented, including one without gain condition, but we presented in [4] a slight improvement to the estimator proposed in [15] where better performance and simpler convergence analysis are obtained. In [21], a global exponential estimator has been presented but the globality has been reached at the cost of breaking the normality constraint of the gravity and magnetic field direction vectors. In that work, this has been fixed by projecting the rotation matrix on SO(3). However, this solution becomes discontinuous and even undefined in the vicinity of singularities. Indeed, the topology of SO(3) implies that an estimator with continuous dynamics cannot be globally stable [7]. Indeed, globality is a desirable feature [3], [11], [6] but sometimes the continuity of the estimation and its dynamics are more important, for example when the continuity of the control is required.

We presented in [5] a simple two-steps tilt estimator dedicated to humanoid robots, but there was only a shallow analysis of the dynamics, no generalization of the estimator to higher-order filtering, and no extension to full attitude. We propose here to extend that work and at the same time the work of [15] and [21] with a set of improved estimators with the same guarantees of almost global convergence. Let us denote $R \in SO(3)$ the attitude we want to reconstruct, and the tilt $x_2 = R^T e_z$ where e_z is a unit vector aligned with the gravitational field. We first introduce a new tilt observer called a "two-step state observer" which operates in two steps: the first one provides an intermediate estimate $\hat{x}_2' \in \mathbb{R}^3$ of x_2 while the second step furnishes the recommended estimate $\hat{x}_2 \in \mathbb{S}^2$ of x_2 based on $\hat{x}_2'$. The expected efficiency of this estimator comes from the decoupling of the two constitutive steps: the first one ensures global exponential convergence of $\hat{x}_2'$ towards x_2 while the second one is an $\mathbb{S}^2$-constrained complementary-filter estimation providing continuous dynamics and better robustness to disturbances. We present then an estimator for the full attitude that can be adapted to our confidence in the magnetometer. All the estimators have a simple structure, proof of asymptotic convergence, and good overall performance. The quality of the estimate is evaluated by the comparative simulation with state-of-the-art solutions.

B. Frames, measurements and definitions

We denote $\mathcal{W}$ as the world frame and $\mathcal{L}$ as the local frame of the sensor. This attitude estimation has to rely on an IMU consisting of a three-axial accelerometer, gyrometer (also called gyroscope), and magnetometer, and using a measurement of the velocity of the sensor. The accelerometer gets a measurement of the inertial linear inertial forces exerted on the sensor, which can be seen as an indistinct sum of the gravitational field and the linear acceleration of the sensor, the gyrometer provides a measurement of the angular velocity ω of the IMU and the magnetometer provides a measurement of the unit vector along the Earth's magnetic field. All these signals, respectively denoted y_a, y_g and y_m, are expressed in the sensor frame $\mathcal{L}$ [23]. The velocity sensor provides the linear velocity v of the local frame $\mathcal{L}$ with respect to the world $\mathcal{W}$ but expressed in $\mathcal{L}$, we denote this measurement y_v. That is

$$y_v = v, \tag{1}$$
$$y_g = \omega, \tag{2}$$
$$y_a = S(\omega)v + \dot{v} + g_0 R^T e_z, \tag{3}$$
$$y_m = R^T m, \tag{4}$$

R, g_0, e_z and m are respectively the 3×3 matrix in SO(3) representing the orientation of the IMU with respect to the world $\mathcal{W}$, the standard gravity constant, a unit vector collinear with the gravitational field, expressed in $\mathcal{W}$ and directed upward, and a unit vector aligned with the earth's magnetic field expressed in $\mathcal{W}$. Note that we consider a flat earth model where the gravitational and magnetic fields are constant with translations. Finally, ω is the angular velocity of the sensor expressed in $\mathcal{L}$ such that

$$\dot{R} = RS(\omega), \tag{5}$$

where the function S is the skew-symmetric matrix operator allowing to perform cross-product. Some common properties of this operator, used for the developments in this paper, are provided in Appendix VII-A.

We introduce then some notations. For $n \geq 1$, define $\Upsilon_n \triangleq \mathbb{R}^{3n} \times \mathbb{S}_{e_z}$ and $\Upsilon_n^* \triangleq \mathbb{R}^{3n} \times \mathbb{S}_{e_z}^*$ with $\mathbb{S}_{e_z} \triangleq \left\{ z \in \mathbb{R}^3 | \, (e_z - z) \in \mathbb{S}^2 \right\}$ and $\mathbb{S}_{e_z}^* \triangleq \mathbb{S}_{e_z} \setminus \{2e_z\}$.

Also, we will say that a dynamical system (D) $\dot{x} = f(x)$ defined on a differential manifold X is *almost globally asymptotically stable with respect to an equilibrium point* x_0 *of* f if (D) is (Lyapunov) locally stable with respect to x_0 and there exists an open and dense subset X_1 of X such that every trajectory starting in X_1 converges asymptotically to x_0.

We define the tilt as the image of e_z, the global gravity field expressed in $\mathcal{L}$, the local frame of the sensor and we note it x_2, formally defined as

$$x_2 \triangleq R^T e_z. \tag{6}$$

This variable lies in the unit sphere $\mathbb{S}^2$ centered at the origin, which is a 2D manifold and is then insufficient to

rebuild the whole attitude R. We call the remaining degree of freedom "yaw". Despite the similar name and meaning, note that this yaw is different from the yaw angle defined by the roll, pitch, and yaw Euler angles because it is not properly an angle and we do not specify the order among the horizontal vectors.

There is no formal definition of the yaw angle that is singularity-free. Nonetheless, the yaw may contribute for example to complement the tilt estimation with the value of $R^T m$ such as measured by y_m, and then we can obtain the full attitude R [25].

As explained in the introduction, there are many cases where the magnetometer provides unreliable measurements or is completely unavailable. Nonetheless, we show in Section III that, in this case, the tilt is still observable with good convergence guarantees.

In Section IV we show the case where the magnetometer is available and the full rotation matrix R can be reconstructed. In fact, the presence of the magnetometer provides us with some redundancy also for tilt observation and may improve it. However, if the quality of the magnetometer's measurements is too poor it may instead downgrade the quality of the tilt estimation. We show then how to explicitly consider the level of confidence given to the magnetometer. This would define how much the magnetometer interferes with the estimation of tilt while keeping good convergence guarantees for the full attitude.

III. Tilt estimation

In this section, we ignore the signals of the magnetometer, either because it is unavailable or because the magnetic field is not steady. In this case, the whole orientation cannot be observed. Nevertheless, we show hereinafter how we can have an efficient estimation of tilt $x_2 \triangleq R^T e_z$.

We present a novel observer called "Two-steps state observer" which is designed in two steps: the first step provides $\hat{x}_2' \in \mathbb{R}^3$, which is an intermediate estimate of x_2; and the second provides $\hat{x}_2 \in \mathbb{S}^2$, which is the recommended estimate of x_2 based on $\hat{x}_2'$. The expected efficiency of this estimator is that it relies on two stages, the first independent one is given by $\hat{x}_2'$ which is globally exponentially converging to x_2 in an efficient way, and the second is a $\mathbb{S}^2$-constrained complementary-filter estimation providing continuity and better robustness to disturbances. Indeed, the global exponential convergence of the error of the first stage actually leads to the violation of the normality constraint of $R^T e_z$. Furthermore, the simple normalization of this estimation may lead to an undefined output and unbounded time-derivatives when the norm is close to zero. This can cause a problem when the continuity of the estimation is required. A simple solution is to add the second stage to maintain the constraint of the tilt estimation in $\mathbb{S}^2$ while keeping bounded velocities.

A. State definition and dynamics

Let us define the following state variables:

$$x_1 \triangleq v, \tag{7}$$
$$x_2 \triangleq R^T e_z, \tag{8}$$

where $x_1 \in \mathbb{R}^3$ and $x_2 \in \mathbb{S}^2$, with the set $\mathbb{S}^2 \subset \mathbb{R}^3$ being the unit sphere centered at the origin, and defined as

$$\mathbb{S}^2 \triangleq \left\{ x \in \mathbb{R}^3 | \, \|x\| = 1 \right\}. \tag{9}$$

The variable x_1 is measured using y_v, even if it is noisy. On the contrary, x_2 is the tilt that cannot be obtained algebraically from the measurements.

From equations (3) and (7) we get

$$\dot{x}_1 = -S(\omega)x_1 + y_a - g_0 R^T e_z. \tag{10}$$

This, together with the time-differentiation of x_2 using equation (5), provides us with the following state dynamic equations

$$\begin{cases} \dot{x}_1 &= -S(\omega)x_1 + y_a - g_0 x_2, \\ \dot{x}_2 &= -S(\omega)x_2, \end{cases} \tag{11}$$

The system (11) is suitable for observer synthesis.

B. Two-steps first order estimator designed in $\mathbb{R}^3 \times \mathbb{S}^2$

The simplest two-steps estimator can be described as follows,

$$\begin{cases} \dot{\hat{x}}_1 &= -S(y_g)\hat{x}_1 + y_a - g_0 \hat{x}_2', \\ \hat{x}_2' &= -\frac{\alpha_1}{g_0}\left(y_v - \hat{x}_1\right), \\ \dot{\hat{x}}_2 &= -S\left(y_g - \gamma S(\hat{x}_2)\hat{x}_2'\right)\hat{x}_2, \end{cases} \tag{12}$$

where α_1 and γ are positive scalar gains, and $\hat{x}_1$ an intermediate variable. Note that $\hat{x}_1$ is not an estimator for x_1, we use this symbol for better consistency with higher order estimators presented in the next sections.

If the initial value of $\hat{x}_2$ is in $\mathbb{S}^2$, then the dynamics of the last equation ensure that the norm of this vector remains in time constantly equal to one. The initial value for $\hat{x}_1$ on the other side could be anywhere in $\mathbb{R}^3$.

Using the estimation errors defined as $\tilde{x}_2' \triangleq x_2 - \hat{x}_2' = x_2 + \frac{\alpha_1}{g_0}\left(x_1 - \hat{x}_1\right) = p_1$ and $\tilde{x}_2 \triangleq x_2 - \hat{x}_2$, and equation (11) we get the error dynamics as

$$\begin{cases} \dot{p}_1 &= -S(\omega)p_1 - \alpha_1 p_1, \\ \dot{\tilde{x}}_2 &= -S(\omega)\tilde{x}_2 + \gamma S^2\left(\hat{x}_2\right)\left(\tilde{x}_2 - p_1\right). \end{cases} \tag{13}$$

To run the analysis of errors, we set $z_{p_1} = Rp_1$ and $z_2 = R\tilde{x}_2$. Noticing $R\hat{x}_2 = e_z - z_2$, one gets

$$\begin{cases} \dot{z}_{p_1} &= -\alpha_1 z_{p_1}, \\ \dot{z}_2 &= \gamma S^2\left(e_z - z_2\right)\left(z_2 - z_{p_1}\right). \end{cases} \tag{14}$$

These new error dynamics are autonomous and define a time-invariant ordinary differential equation (ODE). If one defines the state $\xi_1 \triangleq (z_{p_1}, z_2) \in \Upsilon_1$ one can write (14) as $\dot{\xi}_1 = F_1(\xi_1)$ where F_1 gathers the right-hand side of (14) and defines a smooth vector field on Υ_1.

We now turn to the convergence analysis of (14) and we get the following.

Theorem 1. *The time-invariant ODE defined by (14) verifies the following*

1) *The state space is equal to Υ_1, it admits two equilibrium points namely the origin $(0,0)$ and $(0, 2e_z)$ and all trajectories of (14) converge to one of the two equilibrium points.*

2) *The system* (14) *is almost globally asymptotically stable with respect to the origin.*
3) *For every compact set* K *of* Υ_1^* *and positive number* $\varrho > 0$*, there exists* (α_1, γ) *such that trajectories of (14) starting in* K *converge exponentially to the origin with an exponential rate larger than or equal to* ϱ*.*

The proof of the theorem is given in Section VII-B.

Remark 2. The estimator for the tilt x_2 operates in two *decoupled* steps: the first one shows that the artificial state $\hat{x}_2'$ estimates x_2 (the dynamics of the error term z_{p_1} are independent of the rest of the system dynamics) and then, in the second step, one brings back $\hat{x}_2'$ on $\mathbb{S}^2$ through $\hat{x}_2$.

C. Two-steps n^{th} order estimator designed in $\mathbb{R}^{3n} \times \mathbb{S}^2$

An interesting way to comprehend the estimator (12) is by noting that the dynamics of $\hat{x}_2'$ have a first-order exponential convergence to x_2 and that the dynamics of $\hat{x}_2$ are a complementary filter of $\hat{x}_2'$. Therefore, we can extend this feature to a higher order of exponential convergence while keeping the same two-step structure tilt estimator. Let $n \geq 2$ be an integer. The n-th order observer is designed on $\mathbb{R}^{3n} \times \mathbb{S}^2$, where n is the order of the filter for the first step of the estimator. Since increasing the order of the linear filtering decreases the gain at higher frequencies, it reduces the effect of the noises on the signals of the accelerometer y_a and the linear velocity y_v.

Define $p_n \triangleq y_v - \hat{x}_1 = x_1 - \hat{x}_1$. Then the two-steps n-th order observer is given by

$$\begin{cases} \dot{\hat{x}}_2' &= -S\left(y_g\right)\hat{x}_2' - \frac{\alpha_1}{g_0}p_2, \\ \dot{p}_i &= -S\left(y_g\right)p_i + p_{i+1},\ (i = 2, \cdots, n-1) \\ \dot{\hat{x}}_1 &= -S\left(y_g\right)\hat{x}_1 + y_a - g_0\hat{x}_2' + \sum_{i=2}^{n}\alpha_i p_i, \\ \dot{\hat{x}}_2 &= -S\left(y_g - \gamma S\left(\hat{x}_2\right)\hat{x}_2'\right)\hat{x}_2. \end{cases} \tag{15}$$

Here, the gains α_i, $(i = 1, \ldots, n)$ are positive and chosen so that the polynomial $s^n + \alpha_n s^{n-1} + \alpha_{n-1}s^{n-2} + \alpha_{n-2}s^{n-3} + ... + \alpha_2 s + \alpha_1$ is Hurwitz. Moreover, $\hat{x}_1$ and $\hat{x}_2$ are estimations of x_1 and x_2 respectively and $\hat{x}_2'$ is an intermediate estimation of x_2. Using the estimation errors defined as $\tilde{x}_1 \triangleq x_1 - \hat{x}_1 = p_n$, $\tilde{x}_2' \triangleq x_2 - \hat{x}_2' \triangleq p_1$ and $\tilde{x}_2 \triangleq x_2 - \hat{x}_2$, we get the error dynamics as

$$\begin{cases} \dot{p}_1 &= -S\left(\omega\right)p_1 + \frac{\alpha_1}{g_0}p_2, \\ \dot{p}_i &= -S\left(\omega\right)p_i + p_{i+1},\ (i = 2, \cdots, n-1) \\ \dot{p}_n &= -S\left(\omega\right)p_n - g_0 p_1 - \sum_{i=2}^{n}\alpha_i p_i \\ \dot{\tilde{x}}_2 &= -S\left(\omega\right)\tilde{x}_2 + \gamma S^2\left(\hat{x}_2\right)\tilde{x}_2 - \gamma S^2\left(\hat{x}_2\right)p_1. \end{cases} \tag{16}$$

To run the error analysis, we set $z_{p_1} \triangleq Rp_1$, $z_{p_i} \triangleq \frac{\alpha_1}{g_0}Rp_i$ $(i = 2, \cdots, n)$ and $z_2 \triangleq R\tilde{x}_2$. Then one gets

$$\begin{cases} \dot{z}_{p_i} &= z_{p_{i+1}},\ (i = 1, \cdots, n-1) \\ \dot{z}_{p_n} &= -\sum_{i=1}^{n}\alpha_i z_{p_i}, \\ \dot{z}_2 &= \gamma S^2\left(e_z - z_2\right)\left(z_2 - z_{p_1}\right). \end{cases} \tag{17}$$

These new dynamics are autonomous as for the first order case and define a time-invariant ordinary differential equation (ODE) on Υ_n. Similarly to the previous state estimator, if one defines the state $\xi_n \triangleq \left(z_{p_1}, \cdots, z_{p_n}, z_2\right) \in \Upsilon_n$, one can write (17) as $\dot{\xi}_n = F_n\left(\xi_n\right)$ where F_n gathers the right-hand side of (17) and defines a smooth vector field on Υ_n.

Note that the first n lines of (17) constitute a separate tilt estimator defined in $\mathbb{R}^{3n}$, which is similar in the case $n = 2$ to the one provided in [21]. We show hereinafter the convergence and the performance of this estimation which is similar to the two-steps first-order tilt estimator.

Theorem 3. *The time-invariant ODE defined by (17) verifies the same statements as in Theorem 1 up to changing* Υ_1 *and* Υ_1^* *by* Υ_n *and* Υ_n^**, the first zero in the equilibrium points now belonging to* $\mathbb{R}^{3n}$ *and* α_1 *changed by* $(\alpha_1, \ldots, \alpha_n)$*.*

The proof of the theorem is given in Section VII-C.

The higher order of the convergence of $\hat{x}_2'$ allows one to improve the robustness of the estimation to noise by increasing the order n, as shown in the simulations of Section V.

Remark 4. In the above construction, it is worth noticing that the gain-coefficients α_i, $1 \leq i \leq n$ can be chosen to be time-varying and the above construction remains unchanged till (17). One can, therefore, use the observer given in [9] which improves the performance of the complementary filter regarding a possible peaking phenomenon and noise. However, in the simulations of this paper, we will take them constant to keep the estimators simple and to make the comparison between them easier.

Note also that if we express the dynamics in the world frame by defining the following change of variable $v_2' = R\hat{x}_2'$, $v_{p_i} = Rp_i$ with $(i = 2, \cdots, n-1)$ and $v_1 = R\hat{x}_1$, we can see that the dynamics become the following

$$\begin{cases} \dot{v}_2' &= -\frac{\alpha_1}{g_0}v_{p_2}, \\ \dot{v}_{p_i} &= v_{p_{i+1}},\ (i = 2, \cdots, n-2) \\ \dot{v}_{p_{n-1}} &= Ry_v - v_1 \\ \dot{v}_1 &= -\alpha_n v_1 + \sum_{i=2}^{n-1}\alpha_i v_{p_i} \\ & \quad -g_0 v_2' + Ry_a + \alpha_n R y_v \end{cases} \tag{18}$$

So the dynamics of this observer are linear with regard to the world-frame expressions of the accelerometer y_a and the velocity sensor y_v. Using Laplace transform we get that

$$\begin{aligned} \mathscr{L}(v_2') = &\frac{\alpha_1}{g_0\left(s^n + \sum_{i=1}^{n}\alpha_i s^{i-1}\right)}\mathscr{L}(Ry_a) \\ &- \frac{\alpha_1 s}{g_0\left(s^n + \sum_{i=1}^{n}\alpha_i s^{i-1}\right)}\mathscr{L}(Ry_v) \end{aligned} \tag{19}$$

where s is the Laplace complex variable and $\mathscr{L}(\cdot)$ is the Laplace transform operator. The analysis of the convergence resorts then to classic linear control theory. Nevertheless, hints on gain tuning are presented at the end of Section IV.

We present the advantages that we associate to these two-step observers over classic ones in Section III-D. But before, we wish to report, hereinafter, the improvements of the estimator presented in [15] that we proposed in [4]. This estimator's design is constituted with an estimate of x_1 used directly to produce the estimate of x_2, so we call it a *one-step* estimator.

D. Two-steps vs one-step state observers

We present here a comparison of the proposed two-step observers with the classic one-step observers. Therefore we start by reminding the reader about these observers and then discussing the differences and advantages of the newly proposed method. So, first, we present a tilt observer that we proposed initially in [4], and which is a slight improvement of the estimator proposed in [15]. It is designed in $\mathbb{R}^3 \times \mathbb{S}^2$ in one step by using the available measures y_g, y_a and y_v and is given by

$$\begin{cases} \dot{\hat{x}}_1 &= -S(y_g)\hat{x}_1 - g_0\hat{x}_2 + y_a + \alpha\tilde{x}_1, \\ \dot{\hat{x}}_2 &= -S(y_g + \gamma S(\hat{x}_2)\tilde{x}_1)\hat{x}_2, \end{cases} \tag{20}$$

where α and γ are positive scalar gains which verify the condition $\gamma g_0 \leq \alpha^2$ and $\hat{x}_1$, $\hat{x}_2$ are the estimations of x_1 and x_2, and $\tilde{x}_1 \triangleq x_1 - \hat{x}_1$.

The observer proposed in [15] is recalled as

$$\begin{cases} \dot{\hat{x}}_1 &= -S(y_g)\hat{x}_1 - g_0\hat{x}_2 + y_a + k_1^v\tilde{x}_1 - k_2^v S^2\left(\hat{x}_2\right)\tilde{x}_1, \\ \dot{\hat{x}}_2 &= -S(y_g + k_1^r S(\hat{x}_2)\tilde{x}_1)\hat{x}_2, \end{cases} \tag{21}$$

where k_1^v, k_2^v and k_1^r are positive scalar gains which verify the condition $k_1^r g_0 \leq k_1^v k_2^v$.

Our proposed observer of (20) could be seen as a special case of (21) since it can be obtained by taking $k_2^v = 0$, $k_1^v = \alpha$, $k_1^r = \gamma$ and the condition on the gains becomes $k_1^r g_0 \leq \left(k_1^v\right)^2$ instead of $k_1^r g_0 \leq k_1^v k_2^v$. However, in [15], the gains are required to be positive for their proof of convergence to hold, and this is not respected with (20).

Using the errors $\tilde{x}_1$ and $\tilde{x}_2 \triangleq x_2 - \hat{x}_2$ as well as $\omega = y_g$, a time-differentiation of these expressions provides us with the following error dynamics (for the observer (20)):

$$\begin{cases} \dot{\tilde{x}}_1 &= -S(\omega)\tilde{x}_1 - \alpha\tilde{x}_1 - g_0\tilde{x}_2, \\ \dot{\tilde{x}}_2 &= -S(\omega)\tilde{x}_2 - \gamma S^2(\hat{x}_2)\tilde{x}_1, \end{cases} \tag{22}$$

The error dynamics of the observer of (21) are given by

$$\begin{cases} \dot{\tilde{x}}_1 &= -S(\omega)\tilde{x}_1 - \alpha\tilde{x}_1 - g_0\tilde{x}_2 + k_2^v S^2\left(\hat{x}_2\right)\tilde{x}_1, \\ \dot{\tilde{x}}_2 &= -S(\omega)\tilde{x}_2 - \gamma S^2(\hat{x}_2)\tilde{x}_1, \end{cases} \tag{23}$$

To run the analysis of errors, we define $z_i \triangleq R\tilde{x}_i$. We notice also that $R(\tilde{x}_2 + \hat{x}_2) = e_z$ which leads to $R\hat{x}_2 = e_z - z_2$. Thus, for (20), we obtain these new error dynamics of our proposed observer

$$\begin{cases} \dot{z}_1 &= -\alpha z_1 - g_0 z_2, \\ \dot{z}_2 &= -\gamma S^2(e_z - z_2)z_1, \end{cases} \tag{24}$$

We do the same for the observer (21), getting the error dynamics as

$$\begin{cases} \dot{z}_1 &= -\alpha z_1 - g_0 z_2 + k_2^v S^2\left(e_z - z_2\right) z_1, \\ \dot{z}_2 &= -\gamma S^2\left(e_z - z_2\right) z_1. \end{cases} \tag{25}$$

These new error dynamics are autonomous. Moreover, for observer (20), almost global asymptotic stability with respect to the origin $(0, 0)$ is obtained with the gain condition $\gamma g_0 \leq \alpha^2$ and the proof is conducted in the same way as in [15] by considering the Lyapunov function candidate given by

$$V \triangleq \frac{\left\|\alpha z_1 + g_0 z_2\right\|^2}{2} + g_0^2 \frac{\left\|z_2\right\|^2}{2}. \tag{26}$$

The time derivative of (26) in view of (24) yields

$$\begin{aligned} \dot{V} = &-\alpha\left(1 - G_0\right)\left\|\alpha z_1 + g_0 z_2\right\|^2 \\ &+ \alpha g_0^2 G_0 z_2^T S^2(e_z) z_2 \\ &- \alpha G_0\left(\left(\alpha z_1 + g_0 z_2\right)^T\left(e_z - z_2\right)\right)^2, \end{aligned} \tag{27}$$

where $G_0 = \frac{\gamma g_0}{\alpha^2} \leq 1$. This Lyapunov function makes the convergence analysis easier than the one given in [15].

The estimators of (20) and (21) are "one-step" observers, as opposed to the two-step observers of the previous developments. It means that they directly track a normalized estimate $\hat{x}_2$ using the estimation error on $\hat{x}_1$. This is why they are structurally different. Nevertheless, there are similarities with the second-order version of (15): the dynamics of $\hat{x}_1$ are identical if we replace $\hat{x}_2'$ by $\hat{x}_2$, and the dynamics of $\hat{x}_2$ in (20) are the projection of the dynamics of $\hat{x}_2'$ in (15) on the normality constraint. Let us discuss now the core differences between our new two-step tilt estimator and one-step ones. Compared to one-step estimators, the price we pay with two-step ones is the intermediate estimate $\hat{x}_2'$, making the observer slightly more complex. But this intermediate estimate has the advantage of not being constrained to $\mathbb{S}^2$ anymore. This is clearly put forward when one compares the error dynamics given by (14) and (23). The decoupling in (14) between the errors z_{p_1} and z_2 not only allows one to have better convergence than (21) (much simpler convergence analysis, simple stability conditions on the gains and arbitrary rate of exponential convergence) but also to improve the robustness of the estimation to noise.

The second major reference for tilt estimation is that of [21] where the authors provide an estimator in $\mathbb{R}^3 \times \mathbb{R}^3$ instead of $\mathbb{R}^3 \times \mathbb{S}^2$ (cf. the variables $\hat{v}$ and $\hat{\gamma}$). The error system turns out to be (essentially) linear and time-invariant with, therefore, the best convergence properties. They extended this method to full attitude R estimation with the help of magnetometers using the TRIAD method [25]. However, the tilt estimator $\hat{\gamma}$ does not belong to $\mathbb{S}^2$ and that may create singularity issues, for example when $\hat{\gamma}$ is close to zero.

The design of our tilt estimator $\hat{x}_2$ aims at combining the good convergence properties of the tilt estimator of [21] with the fact that it remains on $\mathbb{S}^2$, similarly to the tilt estimator of [15] providing good behavior and better noise filtering. This effect will be presented in Section V.

Finally, it is interesting to relate our two-step solution to one estimator presented in [13] where a GPS-aided attitude estimation features an intermediate rotation matrix that is not constrained to be orthogonal. Besides the different nature of the problem treated in that paper, one big difference is that their intermediate estimate does not converge to the desired state to observe. Therefore, the tracking has to take into account additional inputs to compensate for these biases.

IV. Attitude estimation observer

The measurements of the magnetometer provide the direction of the magnetic field expressed in the local frame of the sensor. Usually, most of the measurement is constituted with the Earth's natural magnetic field, which

provides bi-dimensional data on the attitude of the sensor. This gives us enough inputs to reconstruct the full attitude and having then some redundancy with the accelerometer for tilt estimation. However, sometimes due to the proximity of sources of interference, the magnetometer's measurements could lack the necessary reliability to let it influence the critical tilt estimation, but remains the best measurement available to reconstruct the orientation around the vertical direction. To deal with this issue we propose an estimator that allows us to tune how much we wish the magnetometer to interfere with tilt estimation.

A. Design of the attitude observer

Let $\hat{R} \in SO(3)$ denote the estimate of R. In order to take advantage of the estimator of x_2 designed into $\mathbb{R}^3$ given by (15) and the attitude estimator proposed by Mahony et. al [16], we propose the following non-linear attitude observer

$$\begin{cases} \dot{\hat{R}} &= \hat{R}S(y_g - \sigma), \\ \sigma &= \rho_1 S(\hat{R}^T e_z)\hat{x}_2' + \rho_2 S(\hat{R}^T m) y_m \\ &\quad + \mu \hat{R}^T e_z \left(\hat{R}^T e_z\right)^T S\left(\hat{R}^T m\right) y_m. \end{cases} \tag{28}$$

where ρ_1, ρ_2 and μ are positive scalar gains and $\hat{x}_2'$ is given by the first stage of any order of the two-step tilt estimator from Section III, for example with (12).

In the case where $\rho_2 = 0$, we recover an estimate of the total rotation with decoupled tilt in an essentially similar way as that of [15] where the magnetometer does not influence the tilt. On the contrary, if $\mu = 0$, the corresponding estimator is closer to that of [16] and the estimator fully uses the redundancy.

Let $\tilde{R} = R\hat{R}^T$ be the attitude estimation error. A time-differentiation of the expression of (28) and the use of equation (14) provides us with the following error dynamics:

$$\begin{cases} \dot{z}_{p_1} &= -\alpha_1 z_{p_1}, \\ \dot{\tilde{R}} &= \tilde{R} S\left(\tilde{\sigma}\right), \end{cases} \tag{29}$$

where $\tilde{\sigma}$ is given by

$$\begin{aligned} \tilde{\sigma} = &\left(I + \frac{\mu}{\rho_2} e_z e_z^T\right)\left(\rho_1 S\left(e_z\right)\tilde{R}^T e_z + \rho_2 S\left(m\right)\tilde{R}^T m\right) \\ &- \rho_1 S(e_z)\tilde{R}^T z_{p_1}. \end{aligned} \tag{30}$$

Using unit-quaternions instead of elements of $SO(3)$, one associates Q and $\hat{Q}$ with the rotations R and $\hat{R}$ respectively, and similarly the unit-quaternion error $\tilde{Q} = (\tilde{q}_0, \tilde{q}) = Q \odot \hat{Q}^{-1}$ with the attitude estimation error $\tilde{R}$. Here, $\tilde{q}_0 \in \mathbb{R}$ and $\tilde{q} \in \mathbb{R}^3$ are the scalar and the vector components of $\tilde{Q}$ respectively. We can, therefore, write

$$\begin{aligned} &\tilde{R} = I + 2\tilde{q}_0 S\left(\tilde{q}\right) + 2S^2\left(\tilde{q}\right), \\ &\rho_1 S\left(e_z\right)\tilde{R}^T e_z + \rho_2 S\left(m\right)\tilde{R}^T m = -2\left(\tilde{q}_0 I - S\left(\tilde{q}\right)\right) W_\rho \tilde{q}, \end{aligned} \tag{31}$$

with $W_\rho \triangleq -\rho_1 S^2\left(e_z\right) - \rho_2 S^2\left(m\right)$ being a positive-definite symmetric matrix ([26], Lemma 2). From the expression of W_ρ, it is easy to show that for each $\rho_1 > 0$ and $\rho_2 > 0$, the three eigenvalues $\lambda_{1\rho}$, $\lambda_{2\rho}$ and $\lambda_{3\rho}$ of W_ρ are distinct due to the fact that $e_z^T m \neq 0$. It is also easy to show that $\lambda_{3\rho}$, the largest eigenvalue of W_ρ verifies $\lambda_{3\rho} = \lambda_{1\rho} + \lambda_{2\rho}$ and that the corresponding unit eigenvector is $v_{3\rho} = \frac{S(e_z)m}{\|S(e_z)m\|}$.

Set $\varpi \triangleq \left(\tilde{q}_0 I - S\left(\tilde{q}\right)\right) W_\rho \tilde{q}$. The error dynamics written as quaternion error dynamics are now given by

$$\begin{cases} \dot{z}_{p_1} = -\alpha_1 z_{p_1}, \\ \dot{\tilde{q}}_0 = \tilde{q}^T\left(I + \frac{\mu}{\rho_2} e_z e_z^T\right)\varpi \\ \qquad + \frac{1}{2}\rho_1 \tilde{q}^T S(e_z)\left(I - 2\tilde{q}_0 S\left(\tilde{q}\right) + 2S^2\left(\tilde{q}\right)\right) z_{p_1}, \\ \dot{\tilde{q}} = -\left(\tilde{q}_0 I + S\left(\tilde{q}\right)\right)\left(I + \frac{\mu}{\rho_2} e_z e_z^T\right)\varpi \\ \qquad - \frac{1}{2}\rho_1 \left(\tilde{q}_0 I + S\left(\tilde{q}\right)\right) S(e_z)\left(I - 2\tilde{q}_0 S\left(\tilde{q}\right) + 2S^2\left(\tilde{q}\right)\right) z_{p_1}. \end{cases} \tag{32}$$

The above equation defines a time-invariant ordinary differential equation (ODE) and, by considering the state $\xi \triangleq \left(z_{p_1}, \tilde{Q}\right)$ and the state space $\Upsilon \triangleq \mathbb{R}^3 \times \mathbb{S}^3$, one can write this equation as $\dot{\xi} = F\left(\xi\right)$ where F gathers the right-hand side of (32) and defines a smooth vector field on Υ. We analyze these dynamics in the next section.

B. Stability analysis

Let us consider the following positive-definite differentiable function

$$V \triangleq \frac{\rho_1^2}{\alpha_1}\|z_{p_1}\|^2 + 2\tilde{q}^T W_\rho \tilde{q}, \tag{33}$$

which is radially unbounded.

Theorem 5. *The time-invariant ODE defined by (32) verifies the following.*

1) *Its equilibrium points are*

$$\begin{aligned} \widetilde{\Omega}_1 &\triangleq \left\{\xi \in \Upsilon \mid \xi = (0, (\pm 1, 0))\right\}, \\ \widetilde{\Omega}_2 &\triangleq \left\{\xi \in \Upsilon \mid \xi = (0, (0, \pm v_{j\rho})),\ j = 1, 2, 3\right\}, \end{aligned}$$

   where $v_{j\rho}$ are unit eigenvectors of W_ρ for $1 \leq j \leq 3$.
2) *All trajectories of (32) converge to one of the equilibrium points defined in item 1.*
3) *The set equilibrium $\widetilde{\Omega}_1$ which corresponds to the equilibrium point $\left(z_{p_1} = 0, \tilde{R} = I\right)$ is asymptotically stable with a domain of attraction containing the domain*

$$V_c \triangleq \left\{\xi = \left(z_{p_1}, \tilde{Q}\right) \in \Upsilon \mid V\left(\xi\right) < 2\lambda_{min}(W_\rho)\right\}. \tag{34}$$

4) *The equilibria of the set $\widetilde{\Omega}_2$ are unstable and the system is almost globally asymptotically stable with regard to $\widetilde{\Omega}_1$.*

The proof is given in Section VII-D.

Remark 6. The magnetic field measurements y_m can also be filtered using an additional unconstrained state on the unit sphere in the same way as done for the tilt to improve robustness to noise.

Remark 7. In the above, we have chosen, for the simplicity of the analysis, to estimate the intermediate state $\hat{x}_2'$ with the two-steps first-order state observer given by (12). One can also rely on the two-steps n^{th} order state observer given in (17). Then the same theorem holds with a similar proof. Indeed, for the corresponding stability analysis, one replaces the $\|z_{p_1}\|^2$ term in the Lyapunov function V given

in (33) by $\psi_n^T P_\alpha \psi_n$ given in (44). Also, in the linearization of the error dynamics around equilibria we replace $-\alpha I$ in the matrix A of (48) with M_α defined in the proof of Theorem 3 in Section VII-C.

C. Hints on gain tuning

There are five kinds of gains in this observer, and while higher gains produce faster convergence, finding appropriate values for real signals may require some skills. Here we present the theories and experimental feedback on how we tend to tune them.

1) α_1 defines the trust mostly in the measurements y_v of the linear velocity but also in the accelerometer's data y_a. If these sources are reliable then high gains will give good performances. If they are not trustworthy, the observer can still be used since the estimator will treat these sources through complementary filtering, but lower gains are recommended.
2) α_i $(i \in 2, ..., n)$ defines the intermediate level of filtering. High values give importance to the linear velocity estimate $\hat{x}_1$ by lowering the related cut-off frequency of the complementary filter. The gains would take intermediate values to average between the gyrometer feedforward and linear-velocity-based correction, depending on the trust we have in the corresponding sensor measurements.
3) γ or ρ_1 defines the final level of filtering of the tilt estimator, high values give more trust in the first-stage estimation $\hat{x}_2'$ and lower ones give more trust in the integration of the gyrometer, producing smoother outputs.
4) ρ_2 defines the trust we have to let the magnetometer measurements y_m influence the tilt estimation. Therefore, it is usually very low.
5) μ defines the impact of the magnetometer measurements y_m on the yaw definition. It is tuned similarly to any nonlinear complementary filter.

V. Simulations

We show hereinafter the results of the estimators in a simulated environment using Mathworks Simulink. This simulation uses a variable adaptive timestep which may seem ideal compared to real uses with limited frequencies. Nevertheless, this kind of observer is shown to produce stable feedback in a closed-loop balance controller on real humanoid robots with 500Hz sampling frequency [5].

A. Signal generation and initialization

In this section, we present simulation results showing the effectiveness of the proposed estimators. We generated the signal ω and v with trigonometric functions and generated the trajectory of R by integration (see Figure 1), then we simulated the signals of the accelerometer y_a, the gyrometer y_g and the magnetometer y_m such that $m = \frac{1}{\sqrt{2}}(1, 0, 1)^T$.

These signals were used in two cases, ideal signals and noisy ones. For the noisy signals, Gaussian noises were added to the four measurements, the accelerometer y_a, the gyrometer y_g, the velocity sensor y_v, and the normalized magnetometer y_m to which a stronger noise and a bias have been added to make it unreliable and unsuitable to influence tilt estimation. The detail of the noise properties is summarized in Table I.

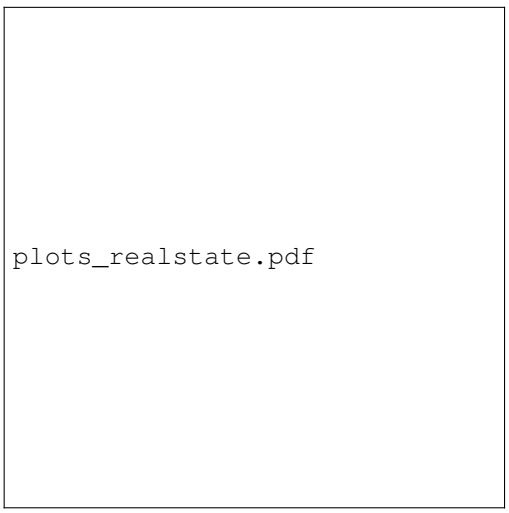

Figure 1. Plot showing the real state of the system. On the top the orientation is shown in Euler angles and on the bottom, the velocity x_1 is shown in its three components.

Measurement	Noise std.	Bias
Accelero. y_a	0.31 m/s^2	$(0\ 0\ 0)^T$
Gyro. y_g	0.1 rad/s	$(0\ 0\ 0)^T$
Magneto. y_m	0.71	$(0.2\ 0.2\ 0.2)^T$
Velocity y_v	0.31m/s	$(0\ 0\ 0)^T$

Table I
Description of the noise parameters.

The same measurement signals are used for all the simulations hereinafter, but we focus separately on the estimation of the tilt alone on one hand and complementing it with yaw estimation on the other. For each tested estimator the initial state was set to $\tilde{R}_3 = 2\left(\frac{m\times e_z}{\|m\times e_z\|}\right)\left(\frac{m\times e_z}{\|m\times e_z\|}\right)^T - I$, which corresponds to an undesired equilibrium. The velocity estimation was initialized to the current sensor value (for instance $\hat{x}_1(0) = x_1(0)$).

B. Comparison between two-steps tilt estimators

The first test is to compare the tilt estimators presented in Section III. Specifically, the first-order, the second-order, and the third-order tilt estimators were compared for the perfect and the noisy measurements. The estimators were designed to have the same (multiple) pole. The parameters are detailed in Table II.

Order	Parameters
1st order	$\gamma = 20$, $\alpha_1 = 2\sqrt{\gamma g_0}$
2nd order	$\gamma = 20$, $\alpha_1 = \left(2\sqrt{\gamma g_0}\right)^2$, $\alpha_2 = 2\left(2\sqrt{\gamma g_0}\right)$
3rd order	$\gamma = 20$, $\alpha_1 = \left(2\sqrt{\gamma g_0}\right)^3$, $\alpha_2 = 3\left(2\sqrt{\gamma g_0}\right)^2$, $\alpha_3 = 3\left(2\sqrt{\gamma g_0}\right)$

Table II
Parameters of tested tilt estimators

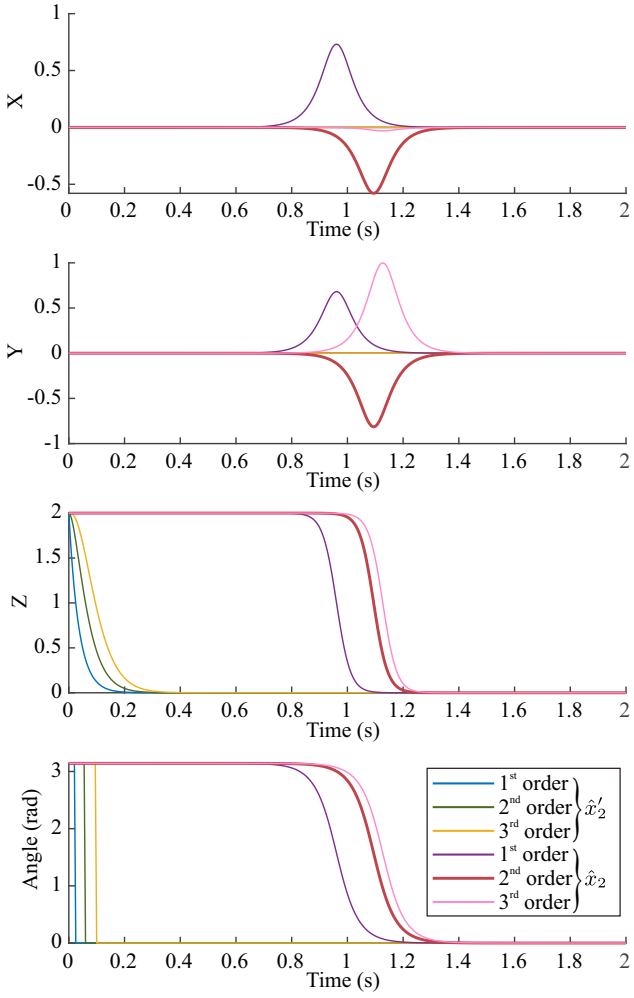

Figure 2. Plot showing the estimation error of the tilt vector x_2 for the three orders of tilt estimators. For each order we show both the intermediate estimation $\hat{x}_2'$ and the final one $\hat{x}_2$. The three top images show the three components of the vector difference error $z_2 = R(x_2 - \hat{x}_2)$ and the bottom plot shows the evolution of the angle between the tilt x_2 and its estimation $\hat{x}_2$.

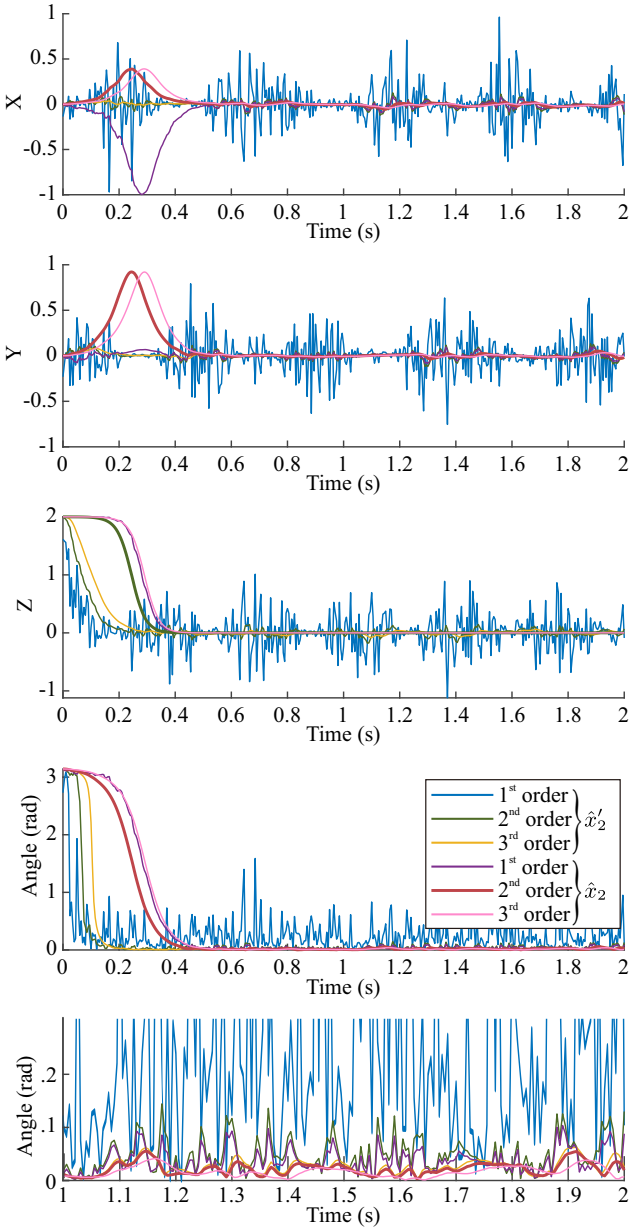

Figure 3. Plot showing the estimation error, in the case of noisy measurements, of the tilt vector x_2 for the three orders of tilt estimators. For each order we show both the intermediate estimation $\hat{x}_2'$ and the final one $\hat{x}_2$. The three top images show the three components of the vector difference error $z_2 = R(x_2 - \hat{x}_2)$=$(X, Y, Z)^T$, the 4th plot shows the evolution of the angle between the tilt x_2 and its estimation $\hat{x}_2$, and the bottom part shows an enlarged plot of the second $[1, 2]$ of the angle error.

The result of the simulation with perfect measurements is shown in Figure 2 where we compare the errors produced by the estimations $\hat{x}_2$, but also the intermediate estimations $\hat{x}_2'$. We see that the intermediate estimation errors converge exponentially to zero while the estimation itself remains in the undesired equilibrium. Later, because of integration noise, the estimation $\hat{x}_2$ could leave the undesired equilibrium and converge quickly to the desired one. For both the intermediate and the final estimate we can see that the first-order estimator is the fastest followed by the other orders.

However, the more interesting case of the noisy one is displayed in Figure 3. We see then that with higher orders of the estimator better filtering is provided. We see also that the sphere constraint of the final estimate $\hat{x}_2$ allows reducing the noise by removing the components which are orthogonal to the constraints. Nevertheless, the difference between the second and third-order versions is small enough to consider that the second-order estimator could be seen as an acceptable compromise between complexity and speed on one side, and filtering quality on the other. This consideration is because the second-order version has a higher sensitivity to high-frequency components of the accelerometer but it is simpler and has a lower delay than the third order.

In the following simulations, we will use this second-order version of $\hat{x}_2'$ in (28) and compare it with state-of-the-art approaches.

C. Comparison between attitude estimators

In this section, five estimators were compared.

1) The attitude estimator described in Section IV with $\rho_2 = 0$, which means it is decoupled to avoid any impact of the magnetometer on the tilt estimation.

We refer to it as hierarchic because it sets a hierarchy between the accelerometer and the magnetometer.

2) The estimator described in Section IV with $\mu = 0$, which means that the magnetometer influences tilt estimation leading to some data redundancy. We will call this estimator *Invariant*.
3) The estimator in $\mathbb{R}^3 \times \mathbb{S}^2$ in Section III-D, and referred to as Benallegue 2017. This one provides only tilt estimation so it does not appear for yaw reconstruction.
4) The estimator designed by Hua et al [15], that they name "Observer 2" in their paper, and that we report in (21). We simply refer to this estimator as Hua 2016.
5) The estimator described in the preprint [21] by Martin et al, named Martin 2016, which is based on two estimators: a tilt estimator equivalent to 2nd order $\hat{x}_2'$ of Sec. III-C and another exponential estimator of the magnetometer. It uses TRIAD-like approach [25] to reconstruct the attitude. The estimation is designed for the tilt to depend only on the accelerometer and the yaw only on the magnetometer.

Each attitude estimator provides a specific tilt estimation. Note that the tilt estimation of the invariant observer is the only one that requires the magnetometer's measurements.

The corresponding gains were designed to have the most equivalent behavior possible, regarding their structure and the considered errors. These estimators, as well as their tilt component and the gains used, are summarized in Table III[1].

1) Perfect measurements: Figure 4 shows the evolution of the tilt error for the five tilt estimators. The first estimator to converge is the one of $\mathbb{R}^3 \times \mathbb{R}^3$, namely 2nd order $\hat{x}_2'$ of Sec. III-C which is not constrained to the unit sphere. This is because the starting position is not an equilibrium point for this vector. However, the normalization of this vector gives a discontinuous trajectory visible at the bottom plot showing the angle error. This is the estimation used in [21]. The next estimator to converge is the invariant one, this is because this estimator uses also the measurements of the magnetometer to speed up the convergence. After that, the estimator in $\mathbb{R}^3 \times \mathbb{R}^3 \times \mathbb{S}^2$ of Section III-C is the next to quickly converge while staying continuous and constrained on the unit sphere. The other estimators converge later, especially the estimation of Hua 2016.

As stated before, there is no singularity-free definition of yaw. Instead, we can study the error in the estimation of the magnetic field direction. Figure 5 shows the evolution over time of the estimation error of the vector $m_p \triangleq e_z \times m \times e_z$ which is orthogonal to e_z but pointing at the same horizontal direction as m. The error is shown as an angle which can be interpreted as a "yaw error" when the tilt error is small. In this figure, we see that the estimation of Martin 2016 [21], is discontinuous at another instant than the discontinuity of the tilt, which means that

[1]The tilt estimation column relates the different estimators to their tilt estimation component and the gains column gives the gain values adopting the notation used in each corresponding cited document.

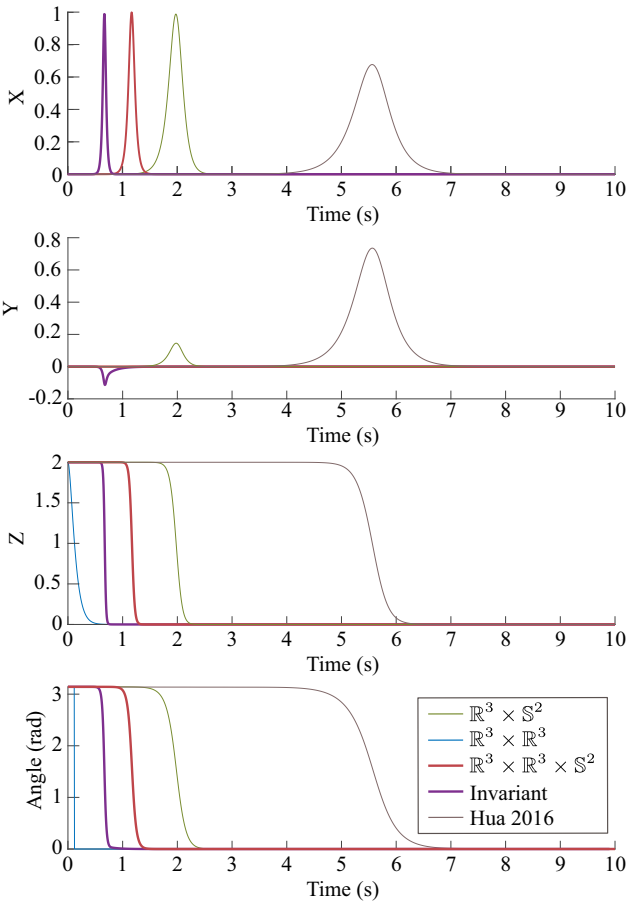

Figure 4. Plot showing the estimation error of the tilt vector x_2 for the five tilt estimators. The three top images show the three components of the vector difference error $z_2 = R\,(x_2 - \hat{x}_2)$ and the bottom plot shows the evolution of the angle between the tilt x_2 and its estimation $\hat{x}_2$. Note that we use the names of the second column of Table III.

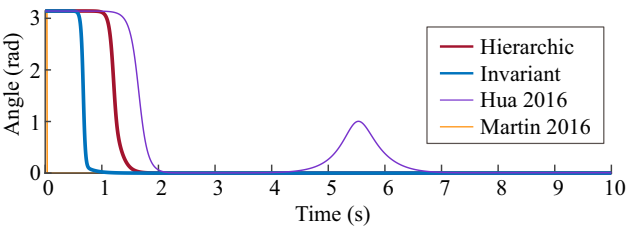

Figure 5. Plot showing the evolution of the angle between $R^T m_p$ and its estimation $\hat{R}^T m_p$ for the four full attitude estimators.

the attitude had two discontinuities while converging. The invariant estimator converges fast, taking full advantage of the redundancy. The hierarchic was the next estimator to converge. We see finally that the estimation error of Hua 2016 moved to zero in the second 2. However, this does not correspond to the convergence of the estimator since it took the tilt estimation 4 more seconds to converge (see Figure 4). This means that it only went from an undesired equilibrium to another one.

Note that some angles increase and then decrease, and this happens because of the tilt estimation converging at the same time and the orthogonality constraint being respected.

2) Noisy Measurements: Figure 6 shows the tilt estimation error with the difference and the angle, similarly

Estimator	Tilt estimation	Gains
Hierarchic (Observer (28) with $\rho_2 = 0$)	$\mathbb{R}^3 \times \mathbb{R}^3 \times \mathbb{S}^2$ (2nd order $\hat{x}_2$ of Sec. III-C)	$\gamma = 20$, $\alpha = 2\sqrt{\gamma g_0} = 28.0143$,
Invariant (Observer (28) with $\mu = 0$)	Invariant (uses magnetometer)	$\mu = 20$ (hierarchic) or $\rho_2 = 20$ (invariant)
Benallegue 2017 [4] of Sec. III-D	$\mathbb{R}^3 \times \mathbb{S}^2$, (provides tilt only)	$\rho_1 = 20$, $\alpha_1 = \gamma g_0$, $\alpha_2 = 2\sqrt{\gamma g_0}$
Hua 2016 [15]	Hua 2016 (observer of Eq. (21))	$k_1^v = k_2^v = \alpha$, $k_1^r = k_2^r = \gamma$
Martin 2016 [21]	$\mathbb{R}^3 \times \mathbb{R}^3$ (2nd order $\hat{x}_2'$ of Sec. III-C)	$L = K = \frac{\alpha}{2}$, $M = \mu$

Table III
SUMMARY OF COMPARED ESTIMATORS IN THE SIMULATIONS.

Tilt estimation	Mean tilt error angle
$\mathbb{R}^3 \times \mathbb{R}^3 \times \mathbb{S}^2$	0.0442 rad
Invariant	0.1543 rad
$\mathbb{R}^3 \times \mathbb{S}^2$	0.0748 rad
Hua 2016	0.1960 rad
$\mathbb{R}^3 \times \mathbb{R}^3$	0.0749 rad

Table IV
AVERAGE TILT ERROR ANGLES DURING 8 SECONDS AFTER THE CONVERGENCE OF THE ESTIMATORS.

Attitude est.	Mean m_p error angle
Hierarchic	0.2374 rad
Invariant	0.2511 rad
Hua 2016	0.2671 rad
Martin 2016	0.3036 rad

Table V
AVERAGE $R^T m_p$ ESTIMATION ERROR ANGLES DURING 8 SECONDS AFTER THE CONVERGENCE OF THE ESTIMATORS.

to Figure 4, with an additional enlarged sample plot of the behavior after the convergence.

From this plot, we see that the noise allowed the estimators to instantly leave the repulsive undesired equilibrium. Then, most estimators except for Hua 2016 converge in less than half a second, the unconstrained $\mathbb{R}^3 \times \mathbb{R}^3$ being the fastest. After the convergence of all the estimators, we see in the enlarged plot that the estimator in $\mathbb{R}^3 \times \mathbb{R}^3 \times \mathbb{S}^2$ has the lowest tilt estimation error angle. The dynamics of the angle error of the estimators in $\mathbb{R}^3 \times \mathbb{R}^3$ and $\mathbb{R}^3 \times \mathbb{S}^2$ have identical local behavior near the desired equilibrium and are almost superimposed in the steady behavior, but we can see in the z-axis plot that the estimator in $\mathbb{R}^3 \times \mathbb{R}^3$ is violating the normality constraint. Interestingly the invariant observer gives worse estimates, that is because it involved unreliable magnetometer measurements which downgrade the performances. We see in Table IV the mean value of the tilt error angle over 8 seconds after the first two seconds of the simulation. The constrained $\mathbb{R}^3 \times \mathbb{R}^3 \times \mathbb{S}^2$ gives the best estimates and the invariant and Hua 2016 both give the worst ones.

Figure 7 shows the evolution of the estimation of $R^T m_p$ together with a zoom on the 6th second of the simulation. We see that the estimations converge in the first second except for Hua 2016. The high level of noise in the magnetometer produces a poor estimation quality, but in the steady behavior, a difference can be shown between observers. This can be quantitatively assessed by looking at Table V showing the average error angle values in the interval [2s,10s]. Martin 2016 has low-quality estimations because the estimation of yaw is performed independently from the measurements of the accelerometer. The other estimators take profit from the better reliability of the tilt estimation and provide a relatively similar level of performance with a slight advantage for the hierarchic estimator.

Note that an intermediate behavior between the hierarchic and the invariant estimator can be obtained by choosing values of μ and ρ_2 appropriately, especially that small values of ρ_2 provide better theoretical convergence guarantees without downgrading excessively the quality of the estimation.

VI. DISCUSSION AND CONCLUSION

We have presented a set of attitude observers targeted toward robotic systems requiring this estimation for dynamical control, such as humanoids and drones. These systems depend mostly on the tilt and need it at high levels of precision and frequency. The solution we propose takes profit from the measurements of an accelerometer, a gyrometer, a magnetometer, and a linear velocity expressed in the local frame.

Each estimator we present is intended to be used in specific cases, mostly related to the reliability of the magnetometer for tilt estimation. Indeed, the magnetometer can be either reliable, unreliable, or totally unavailable. So according to that parameter, we can define how much impact the magnetometer has on the estimation of the tilt. For instance, an invariant complementary filter has a good performance when the magnetometer is reliable but is disturbed when it is not.

Among the estimators, we developed a two-step complementary filter for the tilt that does not use the magnetometer's measurements. Then we augmented this tilt estimator to build a full attitude observer with a tunable magnetometer-to-tilt impact. We have assessed the performance of these estimators through simulations of perfect and noisy measurements.

One additional important contribution of this work lies in the two-step observer itself. The problem was to find a solution to the topological obstruction of the tilt manifold preventing us from stabilizing globally in a "simple" and efficient manner. Our solution is novel from this point of view: we violate the constraint in a "simple" and efficient way, with global exponential stability, then we track this solution with an estimation constrained in this manifold and which is continuous and singularity-free.

Moreover, this solution provides better rejection of disturbances. This is because the topological constraint algebraically filters the disturbances that would violate it, and also because it adds to the observer a local supplementary filtering order, which decreases the influence of high-frequency noises coming from the accelerometer or the linear velocity sensor.

Indeed, there are still open problems that need to be explored. The most prominent one is to deal with the

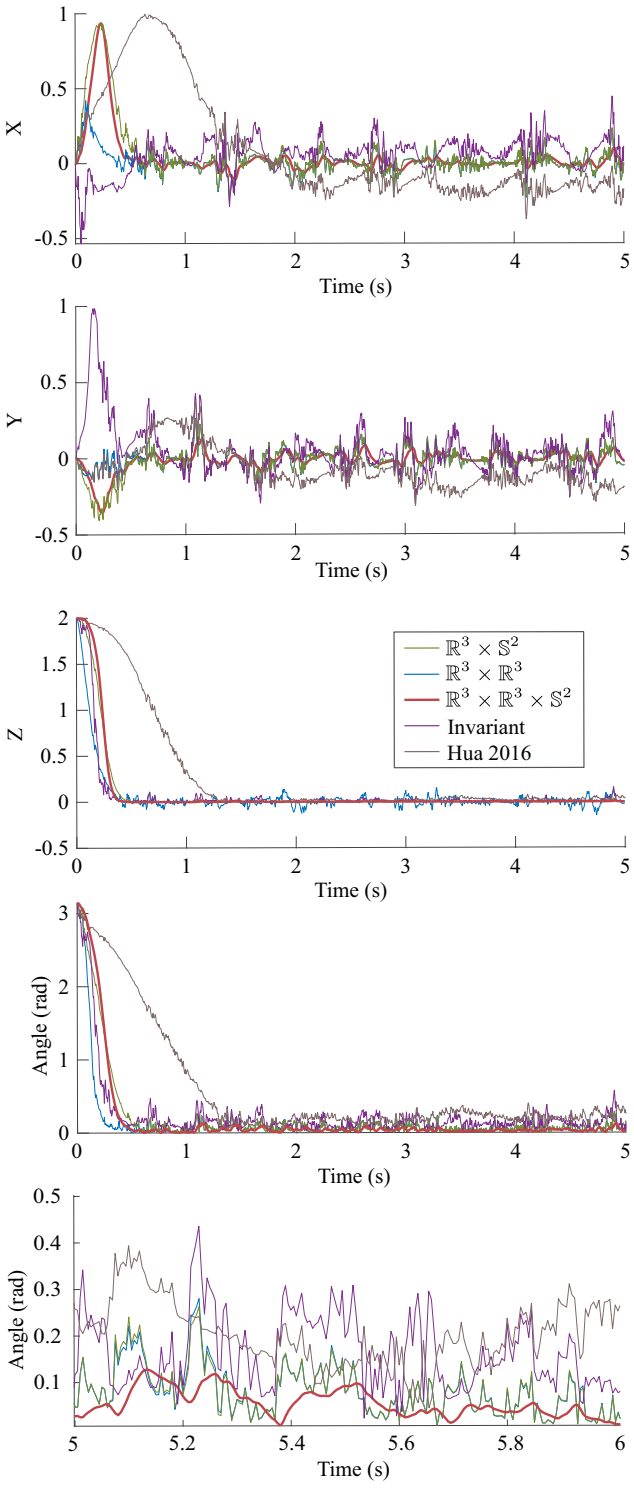

Figure 6. Plot showing the estimation error of the tilt vector x_2 for the five tilt estimators while the measurements were noisy. The three top images show the three components of the vector difference error $z_2 = R\left(x_2 - \hat{x}_2\right)$, the 4th plot shows the evolution of the angle between the tilt x_2 and its estimation $\hat{x}_2$, and the bottom part shows an enlarged plot of the 6th second of the angle error. Note that we use the names of the second column of Table III.

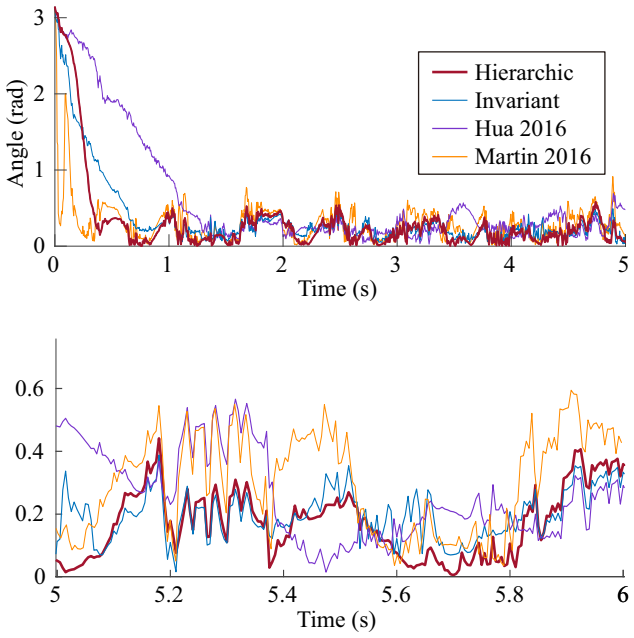

Figure 7. Plot showing the evolution of the angle between $R^T m_p$ and its estimation $\hat{R}^T m_p$ for the five full attitude estimators under noisy measurements.

possible biases in the gyrometer measurements, and that would not only compromise the proofs of convergence but it could decrease the performance of the presented estimators.

Another source of error can be a bias in the measurement of the velocity sensor. If the bias is in the world frame, which could happen because of a steady wind or a moving point of reference, etc. the dynamical equations are similar and the convergence properties of the tilt and the attitude estimations hold still with this estimator. However, if the bias is in the local frame, which can happen because of a defect in the sensor, our proofs don't hold anymore, and identifying and correcting for this bias could be an interesting future development.

VII. Appendix

A. Basic properties

We recall basic properties used in the developments below where v, w and u are vectors and $R \in SO(3)$ is a rotation matrix

$$S\left(v\right) S\left(w\right) = wv^T - \left(v^T w\right) I, \tag{35}$$

$$S\left(v\right) S\left(w\right) S(v) = -\left(v^T w\right) S(v), \tag{36}$$

$$R\left(\prod_{i=1}^{n} S\left(v_i\right)\right) R^T = \prod_{i=1}^{n} S\left(Rv_i\right), \tag{37}$$

$$S\left(S\left(v\right) w\right) = S\left(v\right) S\left(w\right) - S\left(w\right) S\left(v\right), \tag{38}$$

$$= wv^T - vw^T, \tag{39}$$

$$S^3\left(v\right) = -\|v\|^2 S\left(v\right), \tag{40}$$

where I denotes the 3×3 identity matrix.

B. Proof of Theorem 1

One easily checks that the time-invariant ODE defined by (14) leaves invariant the set $\Upsilon_1 = \mathbb{R}^3 \times \mathbb{S}_{e_z}$ because,

along its trajectories, $e_z - z_2 \in \mathbb{S}^2$ keeps a constant norm equal to one. On the other hand, the analysis of the equilibrium points of (14) shows that these are two points: $(0,0)$ and $(0,2e_z)$.

Let us now consider the following positive-definite differentiable function $V_1 : \Upsilon_1 \to \mathbb{R}^+$

$$V_1 \triangleq \frac{\|z_{p_1}\|^2}{2\alpha_1} + \frac{\|z_2\|^2}{2\gamma} \tag{41}$$

then the time derivative of V_1 is given by

$$\dot{V}_1 = -\|z_{p_1}\|^2 + z_2^T S^2(e_z - z_2) z_2 - z_2^T S^2(e_z - z_2) z_{p_1}$$

If we use $w = S(e_z)z_2$, we can write

$$\dot{V}_1 \leq -\begin{bmatrix} \|z_{p_1}\| & \|w\| \end{bmatrix} \begin{bmatrix} 1 & -\frac{1}{2} \\ -\frac{1}{2} & 1 \end{bmatrix} \begin{bmatrix} \|z_{p_1}\| \\ \|w\| \end{bmatrix} \leq 0,$$

and $\dot{V}_1 < 0$ if $(z_{p_1}, w) \neq 0$.

On the other hand, $\dot{V}_1 = 0$ if and only if $z_{p_1} = w = 0$, which is equivalent to (z_{p_1}, z_2) being equal to one of the equilibrium points $(0,0)$ or $(0,2e_z)$. It immediately implies that all trajectories of (14) converge to one of the two equilibria points defined previously.

Recall now that Υ_1 is invariant by (14) and then the second component z_2 of the state remains in $\mathbb{S}_{e_z}$ if it starts there. In addition, note that for $z_2 \in \mathbb{S}_{e_z}$, one has $\|z_2\| \leq \|e_z - z_2\| + \|e_z\| = 2$ and equality holds if and only if $\|z_2\| = 2e_z$. One deduces that for every compact subset K of Υ_1^*, there exists a positive constant $C_1(K) < 1$ such that

$$\|z_2\| \leq 2C_1(K), \text{ for } (z_{p_1}, z_2) \in K. \tag{42}$$

Moreover, for such a compact K, let us prove that there exists $C_2(K) > 0$ such that

$$\|w\| \geq C_2(K)\|z_2\|, \text{ for } (z_{p_1}, z_2) \in K. \tag{43}$$

Indeed, since $z_2 \in \mathbb{S}_{e_z}$ one has $\|z_2\|^2 = 2e_z^T z_2$ and from the definition of w it holds $\|w\|^2 = \|z_2\|^2 - (e_z^T z_2)^2 = e_z^T z_2(2 - e_z^T z_2)$. It implies that $0 \leq e_z^T z_2 \leq 2$ and notice that $e_z^T z_2 = 2$ if and only if $z_2 = 2e_z$. Since $K \subset \Upsilon_1^*$ and is compact, one deduces that there exists $\varepsilon_K > 0$ such that $e_z^T z_2 \leq 2 - \varepsilon_K$ for $(z_{p_1}, z_2) \in K$ and hence $e_z^T z_2 \leq \frac{\|w\|^2}{\varepsilon_K}$. Since $\|w\|^2 \geq \varepsilon_K e_z^T z_2 = 0.5\varepsilon_K \|z_2\|^2$, one deduces (43).

A final important remark is that the set of points of Υ_1 for which V_1 has values less than $V_1(0,2e_z) = 2/\gamma$ is clearly included in the basin of attraction of $(0,0)$ since V_1 is non-increasing along trajectories of (14), regardless of the choice of $\alpha_1, \gamma > 0$.

We next prove the remaining items of Theorem 1. We claim that the basin of attraction of $(0,2e_z)$ is equal to $\mathbb{R}^3 \times \{2e_z\}$, regardless of the choice of $\alpha_1, \gamma > 0$. It is clear that the latter set is included in the required basin of attraction as an instance of the Cauchy-Lipschitz theorem. Similarly one has, along any trajectory $(z_{p_1}(\cdot), z_2(\cdot))$ of (14) starting $(\bar{z}_{p_1}, \bar{z}_2) \in \Upsilon_1$, with $\bar{z}_2 \neq 2e_z$, that $z_2(t) \neq 2e_z$ for every $t \geq 0$. Moreover $z_2(\cdot)$ belongs to the two dimensional manifold $\mathbb{S}_{e_z}$ and the linearized system at $(0,2e_z)$ (tangent to the five-dimensional manifold Υ_1) is $(-\alpha_1)I_{3\times 3} \otimes \gamma I_{2\times 2}$. Together with the fact that $z_{p_1}(t)$ tends to zero as t tends to infinity (and independently of z_2), one deduces that $z_2(\cdot)$ cannot tend to $2e_z$. Using (42), this implies that V_1 takes a value less than $2/\gamma$ and hence the trajectory will tend to $(0,0)$. The claim is proved.

Let K be a compact set in Υ_1^*. By using (43) and the expression of $\dot{V}_1$, one obtains the existence of $C(K) > 0$ such that

$$\dot{V}_1 \leq -C(K)(\|z_{p_1}\|^2 + \|z_2\|^2),$$

for trajectories starting in K (and staying in a compact neighborhood of K in the basin of attraction of $(0,0)$). Then $\dot{V}_1 \leq -2C(K)\min(\alpha_1, \gamma)V_1$. By taking α_1 and γ large enough, one gets the conclusion.

C. Proof of Theorem 3

The argument is similar to that of Theorem 1. For that purpose consider the Hurwitz $n \times n$ matrix in companion form $A_\alpha = J_n - ae_n^T$, where J_n stands for the n-th Jordan block, $a = (\alpha_1, \ldots, \alpha_n)^T$ and $e_n = (0, \cdots, 0, 1)^T$. Then set $M_\alpha = A_\alpha \otimes I_{3\times 3}$ and $\psi_n = (z_{p_1}, \ldots, z_{p_n}) \in \mathbb{R}^{3n}$. Note that the n first equations in (17) can be written $\dot{\psi}_n = M_\alpha \psi_n$. Let P_α be the positive definite real symmetric matrix, unique solution of the Lyapunov equation

$$M_\alpha^T P_\alpha + P_\alpha M_\alpha = -I_{3n\times 3n}.$$

Recall that $\|P_\alpha\| \leq \frac{C}{re_\alpha}$, where C_n is a universal positive constant and $re_\alpha > 0$ is the minimum of $-Re(\lambda)$, where Re stands for the real part and λ is any eigenvalue of the A_α, cf. [12].

One now considers the Lyapunov function

$$V_n = \psi_n^T P_\alpha \psi_n + \frac{1}{2\gamma} z_2^T z_2. \tag{44}$$

We now follow exactly the argument of Theorem 1 and replace $\|z_{p_1}\|$ by $\|\psi_n\|$ to get the conclusion.

D. Proof of Theorem 5

Let us prove the four items of the theorem.

1) The equilibria are calculated by solving the equation $\dot{\xi} = 0$. The solutions of this equation system are given by $(z_{p_1} = 0, \varpi = 0)$. We know from ([26], Lemma 3) that $\varpi = 0$ is equivalent to $(\tilde{q}_0 = \pm 1, \tilde{q} = 0)$ or $(\tilde{q}_0 = 0, \tilde{q} = \pm v_\rho)$ where v_ρ is one of the unit eigenvectors of W_ρ. This completes the proof of item 1.

2) Using the error dynamics given by (32), the time derivative of V in (33) is then given by

$$\dot{V} = -2\rho_1^2 \|z_{p_1}\|^2 + 4\tilde{q}^T W_\rho \dot{\tilde{q}}, \tag{45}$$

which can be developed into

$$\begin{aligned} \dot{V} = &-2\rho_1^2 \|z_{p_1}\|^2 \qquad (46) \\ &- 4\tilde{q}^T W_\rho (\tilde{q}_0 I + S(\tilde{q})) \left(I + \frac{\mu}{\rho_2} e_z e_z^T \right) \varpi \\ &+ 2\rho_1 \tilde{q}^T W_\rho (\tilde{q}_0 I + S(\tilde{q})) S(e_z) \tilde{R}^T z_{p_1}. \qquad (47) \end{aligned}$$

Using the definition of the vector ϖ, we obtain

$$\begin{aligned} \dot{V} = &-2\rho_1^2 \|z_{p_1}\|^2 - 4\|\varpi\|^2 - 4\frac{\mu}{\rho_2}(e_z^T \varpi)^2 \\ &+ 2\rho_1 \varpi^T S(e_z) \tilde{R}^T z_{p_1} \end{aligned}$$

which can be bounded with the following expression

$$\dot{V} \leq -2\rho_1^2 \|z_{p_1}\|^2 - 4\|\varpi\|^2 + 2\rho_1 \|\varpi\| \|z_{p_1}\|. \tag{48}$$

The right-hand side of the above inequality is a quadratic form in $(\|z_{p_1}\|, \|\varpi\|)$ which is negative definite. One easily verifies that $\dot{V} < 0$ if $\xi = \left(z_{p_1}, \tilde{Q}\right)$ is not an equilibrium. Since (32) is autonomous and V is radially unbounded, one can use LaSalle's invariance theorem. Therefore, every trajectory converges asymptotically to a trajectory along which $\dot{V} \equiv 0$.

Since V is non-increasing, $V(\xi) < 2\lambda_{min}(W_\rho)$ at $t = 0$, implies that $\|\tilde{q}(t)\| < 1$ for every $t \geq 0$. Since the trajectory converges to one of the equilibrium points, it must be one with $(z_{p_1} = 0, \tilde{q} = 0)$ which corresponds to $\widetilde{\Omega}_1$ because this is the only one contained in V_c.

4) The undesired equilibria characterized by $\tilde{q}_0 = 0$ are given by $X = (0, (0, v_\rho))$. Let us show that $X = (z_{p_1} = 0, (\tilde{q}_0 = 0, \tilde{q} = v_\rho))$ is unstable. The linearized error dynamics around the unstable equilibrium $X = (0, (0, v_\rho))$ are given by

$$\dot{\xi} = A\xi, \tag{49}$$

where the 7×7 matrix A is equal to $\begin{pmatrix} -\alpha_1 I & 0_{3\times 4} \\ (\star) & F \end{pmatrix}$, and the 4×4 matrix F is given by

$$F = \begin{pmatrix} \lambda_\rho \left(1 + \frac{\mu}{\rho_2}\xi_\rho^2\right) & -\frac{\mu}{\rho_2}\xi_\rho \left(v_\rho^\perp\right)^T (\lambda_\rho I - W_\rho) \\ -\lambda_\rho \frac{\mu}{\rho_2}\xi_\rho \left(v_\rho^\perp\right) & \left(I + \frac{\mu}{\rho_2} v_\rho^\perp \left(v_\rho^\perp\right)^T\right)(\lambda_\rho I - W_\rho) \end{pmatrix},$$

where we have set $v_\rho^\perp = S(v_\rho)\, e_z$ and $\xi_\rho = e_z^T v_\rho$.

We next show that the matrix A has at least one positive eigenvalue for each couple $(\lambda_\rho, v_\rho) \in \{(\lambda_{1\rho}, v_{1\rho}), (\lambda_{2\rho}, v_{2\rho}), (\lambda_{3\rho}, v_{3\rho})\}$ with $\lambda_{1\rho} < \lambda_{2\rho} < \lambda_{3\rho}$.

To see that, let $U = \begin{pmatrix} 1 & \mathbf{0} \\ \mathbf{0} & P \end{pmatrix}$, with $P = \begin{pmatrix} v_1 & v_2 & v_\rho \end{pmatrix}$, be an orthogonal matrix built from v_1, v_2 and v_ρ, the three unit-eigenvectors of W_ρ. Then, an easy computation yields that $U^T F U = \begin{pmatrix} H & \mathbf{0} \\ \mathbf{0} & 0 \end{pmatrix}$, where the zero eigenvalue of F corresponds to the constraint on the quaternion and the 3×3 matrix H is given by (50) in the box on the following page. It is then immediate to notice that $H = (I + \frac{\mu}{\rho_2} zz^T)D$ where $z = (\xi_\rho \;\; v_1^T v_\rho^\perp \;\; v_2^T v_\rho^\perp)^T \in \mathbb{R}^3$ is of norm one and $D = diag(\lambda_\rho, \lambda_\rho - \lambda_1, \lambda_\rho - \lambda_2)$ with λ_1 and λ_2, the two other eigenvalues of W_ρ. Then H is the product of a real symmetric positive definite matrix and a diagonal matrix. Since the positive definite square root of $I + \frac{\mu}{\rho_2} zz^T$ is equal to $C := I + bzz^T$ with $b = \sqrt{1 + \frac{\mu}{\rho_2}} - 1$, one has that H is similar to CDC. That matrix is real symmetric with only real eigenvalues and the largest one, being equal to $\max_{\|x\|=1} x^T CDCx$, is positive, yielding that H admits a positive eigenvalue.

Thus, there exists an unstable manifold of dimension at least one in the neighborhoods of the set $\widetilde{\Omega}_2 = \{(0, (0, \pm v_{j\rho})),\ j = 1, 2, 3\}$, and since all trajectories converge to an equilibrium point, then (32) is almost globally asymptotically stable with respect to the two equilibrium points $\widetilde{\Omega}_1 = \{(0, (\pm 1, 0))\}$, which correspond to $\left(z_{p_1} = 0, \tilde{R} = I\right)$. This completes the proof.

REFERENCES

[1] G. Allibert, D. Abeywardena, M. Bangura, and R. Mahony. Estimating body-fixed frame velocity and attitude from inertial measurements for a quadrotor vehicle. In *2014 IEEE Conference on Control Applications (CCA)*, pages 978–983. IEEE, 2014.

[2] G. Allibert, R. Mahony, and M. Bangura. Velocity aided attitude estimation for aerial robotic vehicles using latent rotation scaling. In *2016 IEEE International Conference on Robotics and Automation (ICRA)*, pages 1538–1543. IEEE, 2016.

[3] Pedro Batista, Carlos Silvestre, and Paulo Oliveira. Sensor-based globally asymptotically stable filters for attitude estimation: Analysis, design, and performance evaluation. *IEEE Transactions on Automatic Control*, 57(8):2095–2100, 2012.

[4] M. Benallegue, A. Benallegue, and Y. Chitour. Tilt estimator for 3D non-rigid pendulum based on a tri-axial accelerometer and gyrometer. In *2017 IEEE-RAS 17th International Conference on Humanoid Robotics (Humanoids)*, pages 830–835. IEEE, nov 2017.

[5] M. Benallegue, R. Cisneros, A. Benallegue, Y. Chitour, M. Morisawa, and F. Kanehiro. Lyapunov-stable orientation estimator for humanoid robots. *IEEE Robotics and Automation Letters*, 5(4):6371–6378, 2020.

[6] S. Berkane, A. Abdessameud, and A. Tayebi. Hybrid attitude and gyro-bias observer design on $so(3)$. *IEEE Transactions on Automatic Control*, 62(11):6044–6050, 2017.

[7] S. P. Bhat and D. S. Bernstein. A topological obstruction to continuous global stabilization of rotational motion and the unwinding phenomenon. *Systems & Control Letters*, 39(1):63–70, 2000.

[8] M. Bloesch, M. Hutter, M. Hoepflinger, S. Leutenegger, C. Gehring, C. D. Remy, and R. Siegwart. State estimation for legged robots - consistent fusion of leg kinematics and imu. In *Proceedings of Robotics: Science and Systems*, Sydney, Australia, jul 2012.

[9] Y. Chitour. Time-varying high-gain observers for numerical differentiation. *IEEE Trans. on Automatic Control*, 47(9), September 2002.

[10] G. F. Franklin, J. D. Powell, and A. Emami-Naeini. *Feedback control of dynamic systems*, volume 3. 2001.

[11] H. F. Grip, T. I. Fossen, T. A. Johansen, and A. Saberi. Globally exponentially stable attitude and gyro bias estimation with application to gnss/ins integration. *Automatica*, 51:158–166, 2015.

[12] R. A. Horn and C.a R. Johnson. *Topics in Matrix Analysis*. Cambridge University Press, 1991.

[13] M.-D. Hua. Attitude estimation for accelerated vehicles using GPS/INS measurements. *Control Engineering Practice*, 18(7):723–732, jul 2010.

[14] M.-D. Hua, T. Hamel, and C. Samson. Riccati nonlinear observer for velocity-aided attitude estimation of accelerated vehicles using coupled velocity measurements. In *2017 IEEE 56th Annual Conference on Decision and Control (CDC)*, pages 2428–2433. IEEE, dec 2017.

[15] M.-D. Hua, P. Martin, and T. Hamel. Stability analysis of velocity-aided attitude observers for accelerated vehicles. *Automatica*, 63:11–15, jan 2016.

[16] R. Mahony, T. Hamel, and J.-M. Pflimlin. Nonlinear complementary filters on the special orthogonal group. *IEEE Transactions on automatic control*, 53(5):1203–1217, 2008.

[17] P. Martin and E. Salaün. An Invariant Observer for Earth-Velocity-Aided Attitude Heading Reference Systems. In *IFAC Proceedings Volumes*, volume 41, pages 9857–9864. Elsevier, jan 2008.

[18] P. Martin and E. Salaün. An invariant observer for earth-velocity-aided attitude heading reference systems. *IFAC Proceedings Volumes*, 41(2):9857–9864, 2008.

[19] P. Martin and E. Salaun. The true role of accelerometer feedback in quadrotor control. In *2010 IEEE International Conference on Robotics and Automation (ICRA)*, pages 1623–1629. IEEE, may 2010.

[20] P. Martin and I. Sarras. A semi-global model-based state observer for the quadrotor using only inertial measurements. In *2016 IEEE 55th Conference on Decision and Control (CDC)*, pages 7123–7128. IEEE, dec 2016.

[21] P. Martin, I. Sarras, M.-D. Hua, and T. Hamel. A global exponential observer for velocity-aided attitude estimation. *arXiv preprint arXiv:1608.07450*, aug 2016.

[22] A. Mifsud, M. Benallegue, and F. Lamiraux. Estimation of Contact Forces and Floating Base Kinematics of a Humanoid Robot Using Only Inertial Measurement Units. In *IEEE/RSJ International Conference on Intelligent Robots and Systems (IROS)*, page 6p., Hamburg, Germany, sep 2015.

[23] P. Ripka and A. Tipek. *Modern Sensors Handbook*, chapter 9.2.1. ISTE. Wiley, 2013.

[24] A. Roberts and A. Tayebi. On the attitude estimation of accelerating rigid-bodies using GPS and IMU measurements. In *IEEE Conference on Decision and Control and European Control Conference*, pages 8088–8093. IEEE, dec 2011.

$$H = \begin{pmatrix} \lambda_\rho \left(1 + \frac{\mu}{\rho_2}\xi_\rho^2\right) & (\lambda_\rho - \lambda_1)\frac{\mu}{\rho_2}\xi_\rho \left(v_1^T v_\rho^\perp\right) & (\lambda_\rho - \lambda_2)\frac{\mu}{\rho_2}\xi_\rho \left(v_2^T v_\rho^\perp\right) \\ \lambda_\rho \frac{\mu}{\rho_2}\xi_\rho \left(v_1^T v_\rho^\perp\right) & (\lambda_\rho - \lambda_1)\left(1 + \frac{\mu}{\rho_2}\left(v_1^T v_\rho^\perp\right)^2\right) & (\lambda_\rho - \lambda_2)\frac{\mu}{\rho_2}\left(v_1^T v_\rho^\perp\right)\left(v_2^T v_\rho^\perp\right) \\ \lambda_\rho \frac{\mu}{\rho_2}\xi_\rho \left(v_2^T v_\rho^\perp\right) & (\lambda_\rho - \lambda_1)\frac{\mu}{\rho_2}\left(v_1^T v_\rho^\perp\right)\left(v_2^T v_\rho^\perp\right) & (\lambda_\rho - \lambda_2)\left(1 + \frac{\mu}{\rho_2}\left(v_2^T v_\rho^\perp\right)^2\right) \end{pmatrix} \tag{50}$$

[25] M. D. Shuster and S. D. Oh. Three-axis attitude determination from vector observations. *Journal of guidance and Control*, 4(1):70–77, 1981.

[26] A. Tayebi, A. Roberts, and A. Benallegue. Inertial vector measurements based velocity-free attitude stabilization. *IEEE Transactions on Automatic Control*, 58(11):2893–2898, Nov 2013.

[27] P. Wawrzyński, J. Możaryn, and J. Klimaszewski. Robust estimation of walking robots velocity and tilt using proprioceptive sensors data fusion. *Robotics and Autonomous Systems*, 66:44–54, 2015.

[28] P.-B. Wieber, R. Tedrake, and S. Kuindersma. *Modeling and Control of Legged Robots*, pages 1203–1234. Springer International Publishing, Cham, 2016.

Mehdi Benallegue.jpg received the ingénieur degree from the Institut National d'Informatique, Algeria, in 2007, the M.Sc. degree from the University of Paris 7, France, in 2008 and the Ph.D. degree from Université de Montpellier 2, France, in 2011 after conducting his research in CNRS/AIST JRL, Tsukuba, Japan, and INRIA Grenoble, France. He has been a postdoctoral researcher at Collège de France and LAAS CNRS, France. He is currently a Researcher with the Joint Robotics Laboratory in AIST, Tsukuba, Japan. His research interests include estimation and control of legged locomotion, biomechanics, neuroscience, and computational geometry.

Abdelaziz Benallegue received his B. Sc. in Electronics from Ecole Nationale Polytechnique d'Alger, Algeria in 1986, his M. Sc. (DEA) in Robotics and Ph.D. in Robotics and Automatic Control from Pierre and Marie Curie University, Paris, France, respectively in 1987 and 1991. He was an associate professor of Automatic control and robotics at the University of Pierre and Marie Curie, Paris 6, France from 1992 to 2002. He joined the University of Versailles St Quentin in 2002 as Professor. His research interests are mainly related to linear and nonlinear control theory including adaptive control, robust control, and neural network learning control, with applications to robot manipulators, humanoids, and aerial vehicles.

Cisneros Rafael received the B.Eng. degree from the University of the Americas - Puebla (UDLA-P), Mexico in 2006, the M.Sc. degree from the Center of Research and Advanced Studies of the National Polytechnic Institute (CINVESTAV-IPN), Mexico in 2009, and the Ph.D. degree from the University of Tsukuba, Japan in 2015. Since then, he has been working at the National Institute of Advanced Industrial Science and Technology (AIST), Japan, from 2015 to 2018 as a post-doc and from 2018 until now as a researcher. He is currently a member of CNRS-AIST JRL (Joint Robotics Laboratory), IRL, AIST. His research interests include torque control, whole-body multi-contact motion control of humanoid robots, multi-body collision dynamics, teleoperation, and tactile feedback.

Yacine Chitour was born in Algeria in 1968. He received the Ph.D. degree from Rutgers, The State University of New Jersey, in 1996. He was with the Mathematics Department of Universite Paris-Sud, Orsay, France, from 1997 to 2004. Since then, he is a Professor of control theory at Universite Paris-Saclay, France, and a member of the Laboratoire des Signaux et Systemes (L2S), CentraleSupelec, and CNRS. He is interested in geometric and optimal control, delay, and switched systems.